Fulde-Ferrell-Larkin-Ovchinnikov superconductivity in the layered organic superconductor β"-(BEDT-TTF)$_4$[(H$_3$O)Ga(C$_2$O$_4$)$_3$]C$_6$H$_5$NO$_2$

S. Uji, Y. Iida, and S. Sugiura
National Institute for Materials Science, Tsukuba, Ibaraki 305-0003, Japan
and Graduate School of Pure and Applied Sciences, University of Tsukuba, Tsukuba, Ibaraki 305-8577, Japan

T. Isono, K. Sugii, N. Kikugawa, and T. Terashima
National Institute for Materials Science, Tsukuba, Ibaraki 305-0003, Japan

S. Yasuzuka
Research Center for Condensed Matter Physics, Hiroshima Institute of Technology, Hiroshima 731-5193, Japan

H. Akutsu and Y. Nakazawa
Department of Chemistry, Graduate School of Science, Osaka University, Toyonaka, Osaka 560-0043, Japan

D. Graf
National High Magnetic Field Laboratory, Tallahassee, Florida 32310, USA

P. Day
Department of Chemistry, University College London, London WC1H 0AJ, United Kingdom

(Received 13 January 2018; published 4 April 2018)

Resistance and magnetic torque measurements are reported in a layered organic superconductor, β"-(BEDT-TTF)$_4$[(H$_3$O)Ga(C$_2$O$_4$)$_3$]C$_6$H$_5$NO$_2$ with $T_c = 4.8$ K, where BEDT-TTF stands for bis(ethylenedithio)tetrathiafulvalene. Because of the large anion between the BEDT-TTF conducting layers, the superconductivity of this salt is highly anisotropic. In magnetic fields parallel to the conducting layers for $T = 0.4$ K, the magnetic torque shows a large diamagnetic signal associated with hysteresis up to ∼21 T, suggesting the upper critical field $H_{c2} \gtrsim 21$ T at 0.4 K. The large reduction of the diamagnetic signal is observed above 16 T, which shows a Fulde and Ferrell and Larkin and Ovchinnikov (FFLO) phase transition. For $T = 0.5$ K, the interlayer resistance has nonzero value in a wide field region up to H_{c2}, arising from the Josephson vortex dynamics. Successive dips in the second derivative curves of the resistance are observed between 16 T and H_{c2}, which are ascribed to the commensurability effect between the Josephson vortex lattice and the order parameter oscillation of the FFLO phase. The commensurability effect is observed only in nearly parallel fields, showing that the FFLO phase is stable in a very limited field angle region. The temperature-field phase diagram is determined.

DOI: 10.1103/PhysRevB.97.144505

I. INTRODUCTION

Layered organic superconductors are modeled as stacks of Josephson junctions since the interlayer coherence length ($\xi_\perp$) is comparable to the layer spacing. Because of the highly two-dimensional (2D) nature, a novel superconducting (SC) phase has been reported to appear in parallel fields sufficiently below the critical temperature T_c [1–17]. In conventional superconductors, the SC order parameter is spatially homogeneous. However, when the superconductivity is in the clean limit and the orbital effect is quenched, a novel SC state where the order parameter oscillates in real space can be stabilized even above the Pauli limit $H_{\rm Pauli}$. This phase was first proposed by Fulde and Ferrell [18] and then by Larkin and Ovchinnikov (FFLO) [19]. For most of the layered organic superconductors, the superconductivity is in the clean limit, and the orbital effect is strongly suppressed in parallel fields. Therefore, layered organic superconductors are recognized as the best candidates for the FFLO phase studies. Among the various candidates, λ-(BETS)$_2$FeCl$_4$ is known to show characteristic vortex dynamics in the FFLO phase. λ-(BETS)$_2$FeCl$_4$ shows a metal-insulator transition at 8 K, which is associated with an antiferromagnetic order [20–22]. The antiferromagnetic insulating phase is broken by applying a magnetic field of about 10 T, and then a paramagnetic metallic phase is recovered [21]. In fields parallel to the conducting *ac* planes, the SC phase is induced in the field range from 17 T to 42 T [2,4,23]. This field-induced SC phase is understood by the Jaccarino-Peter compensation mechanism [24]. In parallel fields, the magnetic flux lines penetrate only the insulating layers, where Josephson vortices (JVs) are formed [Fig. 1(a)]. If the JVs are driven by a perpendicular current, nonzero interlayer resistance is observed even in the SC phase. In λ-(BETS)$_2$FeCl$_4$, the interlayer resistance shows successive dips between 17 T and 25 T in the SC phase [4]. In the FFLO

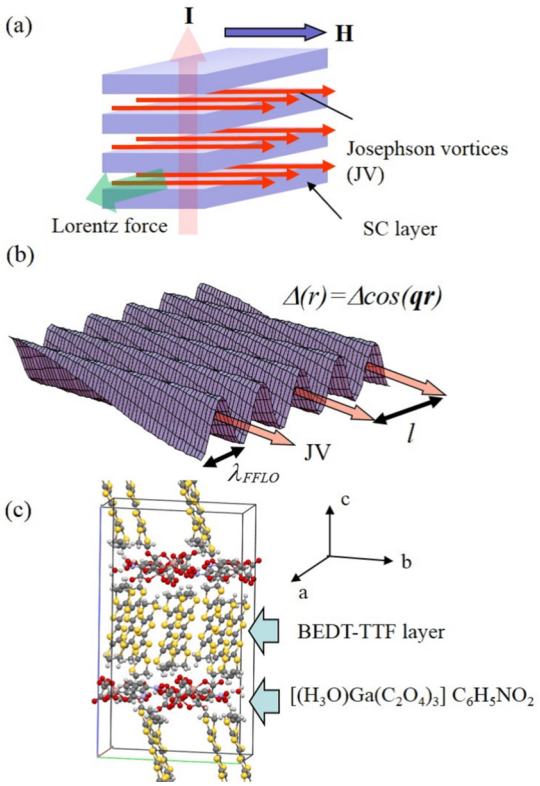

FIG. 1. (a) Schematic of a layered superconductor in parallel magnetic fields. JVs, which are formed in the insulating layers, can be driven by a perpendicular current. (b) Schematics of superconducting order parameter oscillations and JVs in a FFLO phase for a layered superconductor. (c) Crystal structure of β"-(BEDT-TTF)$_4$[$(H_3O)Ga(C_2O_4)_3$]$C_6H_5NO_2$.

phase, the order parameter is given by $\Delta(\mathbf{r}) = \Delta_0\cos(\mathbf{qr})$, where $\mathbf{q}$ is the center-of-mass momentum of the Cooper pair. The dips are interpreted as the magnetic field-dependent commensurability (CM) effect between the wavelength of the FFLO order parameter oscillation $\lambda_{FFLO} = 2\pi/q$ and the JV lattice constant l [4,25]: The dips appear when the JV lattice is collectively pinned by the periodic nodes of the FFLO order parameter [Fig. 1(b)]. On reasonable assumptions, the wavelength λ_{FFLO} is estimated, ranging from 20 to 70 nm. So far, only in λ-$(BETS)_2FeCl_4$, the CM effect has been found. One of the crucial factors for the observation of the CM effect is that the JV lattice is easily driven collectively: The SC state is highly 2D.

The organic superconductor, β"-(BEDT-TTF)$_4$[$(H_3O)Ga(C_2O_4)_3$]$C_6H_5NO_2$ (hereafter β"-salt) has the large anion between the BEDT-TTF layers [Fig. 1(c)] [26], which makes the electronic state highly 2D. The interlayer coherence length $\xi_\perp \approx 1$ nm is comparable to the layer spacing. Therefore, the orbital effect is strongly suppressed in parallel fields and the JVs are pinned very weakly. We have made systematic interlayer resistance and magnetic torque measurements in a wide temperature and field region for the β"-salt and found characteristic field dependence of the interlayer resistance between 16 T and H_{c2}. This is the strong evidence of the CM effect in the FFLO phase. The temperature-field phase diagram in parallel fields and the field angular dependence of the CM effect are also discussed.

II. EXPERIMENTS

Single crystals of the β"-salt were prepared by electrochemical oxidation in an appropriate solvent [26]. The crystal structure is monoclinic ($C2/c$) with the lattice parameters: $a = 1.02782(3)$ nm, $b = 1.98733(6)$ nm, $c = 3.50431(10)$ nm, $\beta = 93.4230(10)^\circ$ at 100 K [Fig. 1(c)]. For the resistance measurements, two gold wires ($\phi 10\mu m$) were attached on both sides of the crystal (conducting ab plane) by carbon paste. The sample resistance R was measured by a conventional four-probe AC technique with an electric current I perpendicular to the conducting layers. The magnetic torque was measured by a microcantilever technique [27]. These experiments were performed by a 31 T resistive magnet at National High Magnetic Field Laboratory, Tallahassee, Florida.

III. RESULTS

A. Resistance

Figure 2 presents the temperature dependence of the interlayer resistance for samples #1 and #2. Both samples show similar behavior except above 200 K. As the temperature decreases, the resistance has a minimum at ~100 K, increases down to 6 K, and then rapidly decreases due to the SC transition. The overall behavior is consistent with previous reports [26,28,29].

The semiconducting behavior of the resistance below ~100 K was first interpreted as the coexistence of insulating and metallic states, which are induced by disorder in the anions and/or the ethylene groups of the BEDT-TTF molecules [28]. Raman spectra show a splitting of the ν_2 mode below 100 K, suggesting a charge order [29]. ^{13}C NMR measurements also show a charge order at low temperatures even in the SC phase [30,31]. On the other hand, the observation of quantum oscillations at low temperatures [28] provides convincing evidence of a metallic state (coherent motion of the electrons) in the BEDT-TTF layers. The semiconducting behavior of the interlayer resistance suggests that the interlayer transfer integral in the charge ordered state is sufficiently smaller than

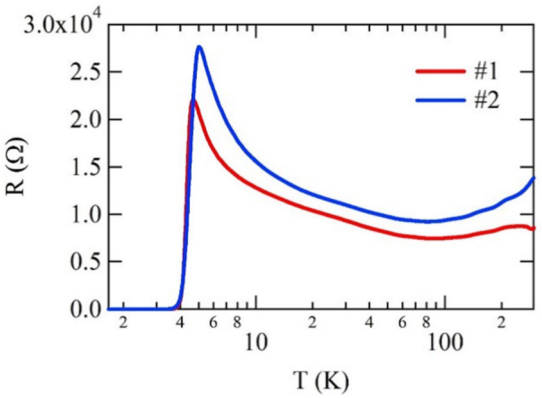

FIG. 2. Temperature dependence of the interlayer resistance for samples #1 and #2.

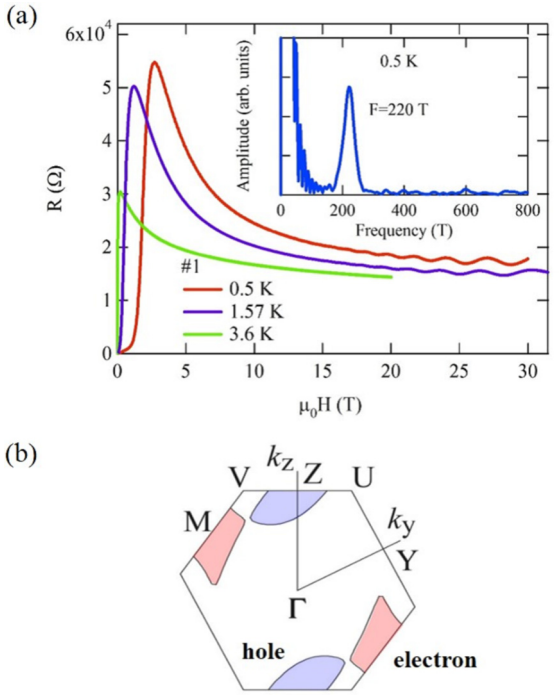

FIG. 3. (a) Interlayer resistance in perpendicular magnetic fields for sample #1. Inset: Fourier transform spectrum of the #SdH oscillation at 0.5 K. (b) Fermi surface calculated by a tight binding approximation. In the first Brillouin zone (hexagonal shape), two closed Fermi surfaces, electron and hole pockets are formed, both of which have the same cross-sectional areas.

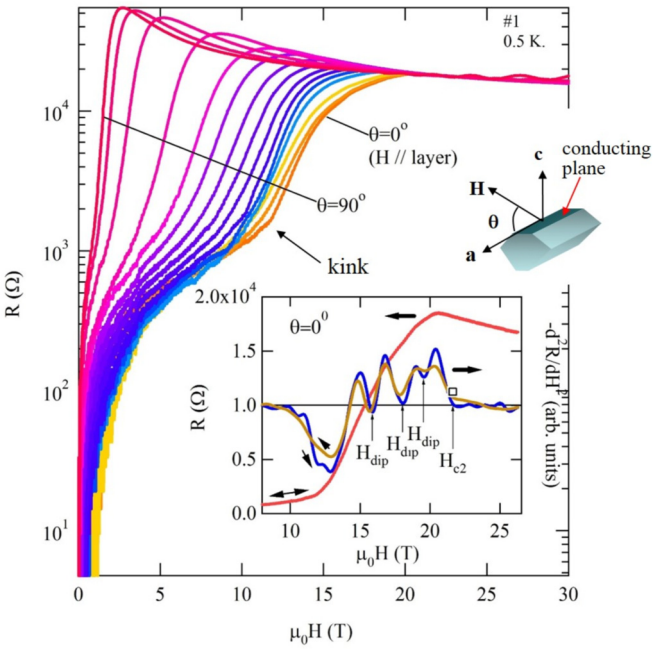

FIG. 4. Semilog plot of the magnetic field dependence of the interlayer resistance at various field angles for sample #1. Inset: Linear plot of the resistance and second derivative curves $-d^2R/dH^2$ for the up and down sweeps at $\theta = 0°$.

k_BT and thermal hopping (incoherent transport) is dominant in the interlayer transport.

Figure 3(a) presents the field dependence of the resistance in perpendicular fields. For $T = 0.5$ K, the resistance rapidly increases above ~1 T, has a sharp peak at ~2.5 T, and then decreases. The decrease of the resistance may suggest that the charge order is suppressed by the field. Above 15 T, where the resistance is almost constant, we observe Shubnikov-de Haas (SdH) oscillations, whose Fourier transform spectrum is shown in the inset. The frequency $F = 220$ T is consistent with the previous report [29]. At higher temperatures, the resistance peak and SdH oscillations are reduced. The band structure calculated by a tight binding approximation is presented in Fig. 3(b) [32,33]. We see two 2D Fermi surfaces, electron and hole pockets. Because of the carrier compensation, both the pockets have the same cross-sectional area, which is consistent with the observation of the single SdH frequency. The SdH frequency of 220 T corresponds to 11% of the Brillouin zone, which well agrees with the band calculation, 11%. If the charge order is formed [31], the Fermi surfaces are reconstructed and then many smaller pockets will be formed, leading to low frequency oscillations. However, the observation of the single frequency shows that the charge order is strongly suppressed by high fields or magnetic breakdown occurs at the Brillouin zone boundary folded by the charge order above 15 T.

Figure 4 presents the field dependence of the resistance at various field angles for $T = 0.5$ K. When the field is parallel to the layers ($H \parallel a, \theta = 0°$), the resistance rapidly increases above ~1 T and has a kink at ~13 T. After that, a broad maximum appears at ~19 T. As the field is tilted, the resistance curve shifts to low fields, associated with the suppression of the kink. The inset of Fig. 4 shows the linear plot of the resistance and second derivative curves $-d^2R/dH^2$ for the up and down sweeps at $\theta = 0°$. We note small structures in the second derivative curves, which are reproducible in both field sweeps. The resistance curve is linear to the field ($-d^2R/dH^2 = 0$) above 21 T but has a downward curvature below it ($-d^2R/dH^2 > 0$), where H_{c2} can be defined. This H_{c2} value is consistent with the magnetic torque data, as shown later. Below 21 T, we see three sharp dips, denoted by $H_{\rm dip}$. The rather broad dip at ~13 T is due to the upward curvature around the kink.

Figure 5 presents the second derivative curves of the resistance at various angles. For $\theta \approx 0°$, we see the dip structures between 16 T and 20 T. As the field is tilted, the dips are suppressed and disappear for $\theta \gtrsim 3°$. The SdH oscillations are observed at high fields for $\theta \gtrsim 50°$.

Figures 6(a) and 6(b) present the magnetic field dependence of the interlayer resistance at various field angles at 1.64 K and 3.6 K, respectively. For $\theta = 0°$ at 1.64 K, the resistance has a similar kink at ~8 T and a maximum at ~16 T. As the field is tilted, the resistance curve shifts to low fields. We also see a dip in the second derivative curve $-d^2R/dH^2$ as indicated by an arrow in the inset. At 3.6 K, we see a gradual increase of the resistance and a maximum, but no dip in $-d^2R/dH^2$ [inset of (b)].

Figure 7 presents the angular dependence of H_{c2} and $H_{\rm dip}$ at three different temperatures. At these temperatures, H_{c2} has a maximum at $\theta = 0°$ and decreases as the field is tilted. The red and blue curves show the simulations for the Tinkham 2D [34] and anisotropic 3D models [35], respectively. The

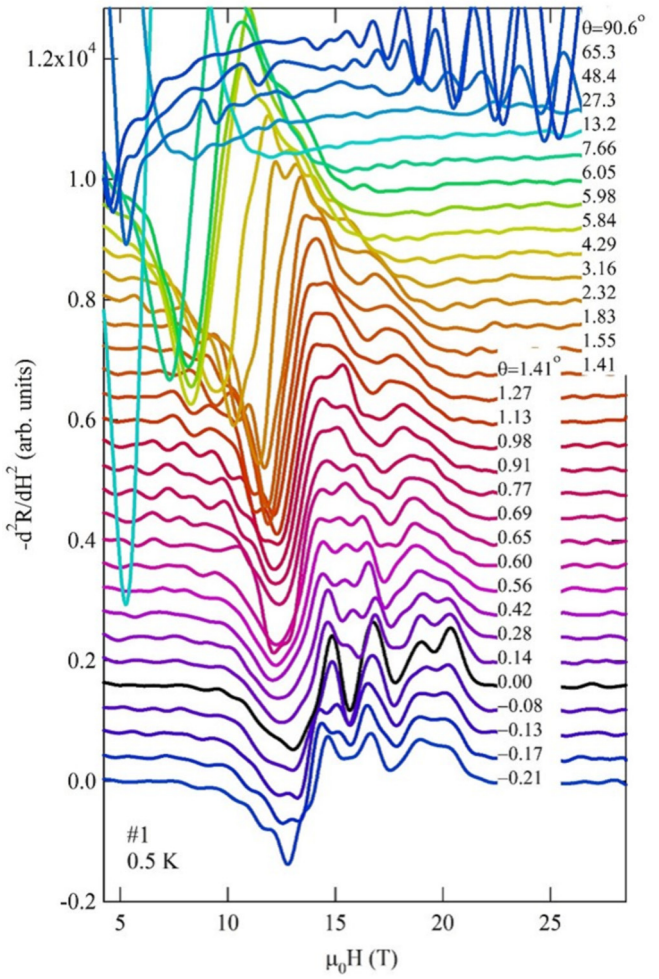

FIG. 5. Second derivative curves $-d^2R/dH^2$ for the down sweep at various field angles. The curves are shifted for clarity.

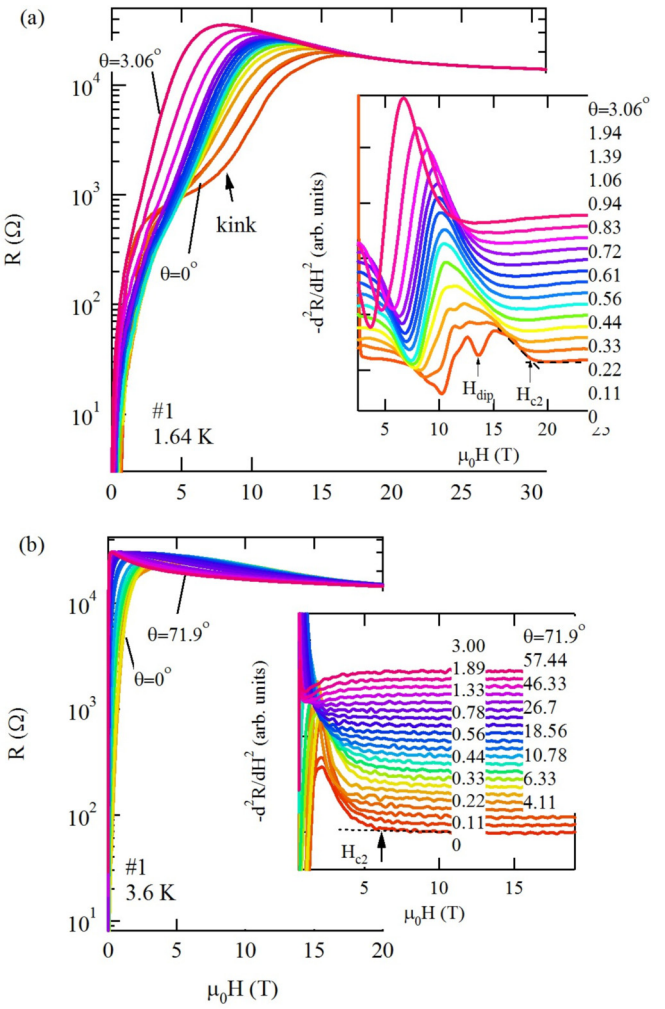

FIG. 6. Semilog plots of the resistance at (a) 1.64 K and (b) 3.6 K. Insets: Second derivative curves $-d^2R/dH^2$ of the main panel data. The curves are shifted for clarity.

2D model apparently reproduces the experimental results much better than the 3D model. At 1.6 and 3.6 K, we see deviations from the simulations near zero degrees. The reason will be due to ambiguity of the definition of H_{c2}; the H_{c2} values inevitably include rather large ambiguity, arising from the vortex flow resistance, superconducting fluctuation, and background magnetoresistance behavior. At 0.5 K, the dips appear at high fields only for $\theta < 2^\circ$. Although the data points of $H_{\rm dip}$ are rather scattered, we see four series of the dips, two of them are independent of the angle and the others decrease with angle. At 1.6 K, we see only a single dip for $\theta = 0^\circ$.

Figure 8(a) presents the magnetic field dependence of the resistance at various temperatures. As temperature increases, both the kink and maximum shift to low fields. In the second derivative curves [Fig. 8(b)], we can similarly define $H_{\rm dip}$ and H_{c2} as indicated by arrows, both of which decrease with increasing temperature. The dips are suppressed with increasing temperature and not evident above 2.5 K.

B. Magnetic torque

The magnetic torque is expressed as $\tau = \mu_0 \mathbf{M} \times \mathbf{H}$, where M is the magnetization. For highly 2D superconductors, when the field is nearly parallel to the layers and the parallel field $H_\parallel$ is much larger than the lower critical field, the magnetic torque is reduced to the formula, $\tau \simeq \mu_0 M_\perp H_\parallel$ [36], where $M_\perp$ is the perpendicular magnetization. Therefore, $\tau/H_\parallel$ directly gives the magnetization curve $M_\perp(H_\perp)$.

The torque curves as a function of field are plotted in Fig. 9 when the field is nearly parallel to the layers. We observe large hysteresis in a wide field region, which is ascribed to the vortex pinning in the SC layers. Above ~21 T, the torque curve becomes reversible, where the irreversibility field $H_{\rm irr}$ can be defined (inset of Fig. 9). For $\theta \approx 0^\circ$, the torque signal is very small ($M_\perp \approx 0$), showing almost all the flux lines penetrate the insulating layers. The irreversible behavior clearly shows the bulk superconductivity up to $H_{\rm irr}$. Since the gradual change of the torque curves, we cannot define H_{c2}, which should be larger than $H_{\rm irr}$. The $H_{\rm irr}$ value approximately agrees with H_{c2} determined by the resistance measurements.

Typical torque curves for two different rotations at 0.4 K are shown in the inset of Fig. 10. A sharp feature around $\theta = 0^\circ$ arises from the SC transition, which is superimposed on a smooth background given by a $\cos(2\theta)$ curve. Large hysteresis between the two rotations is ascribed to the vortex

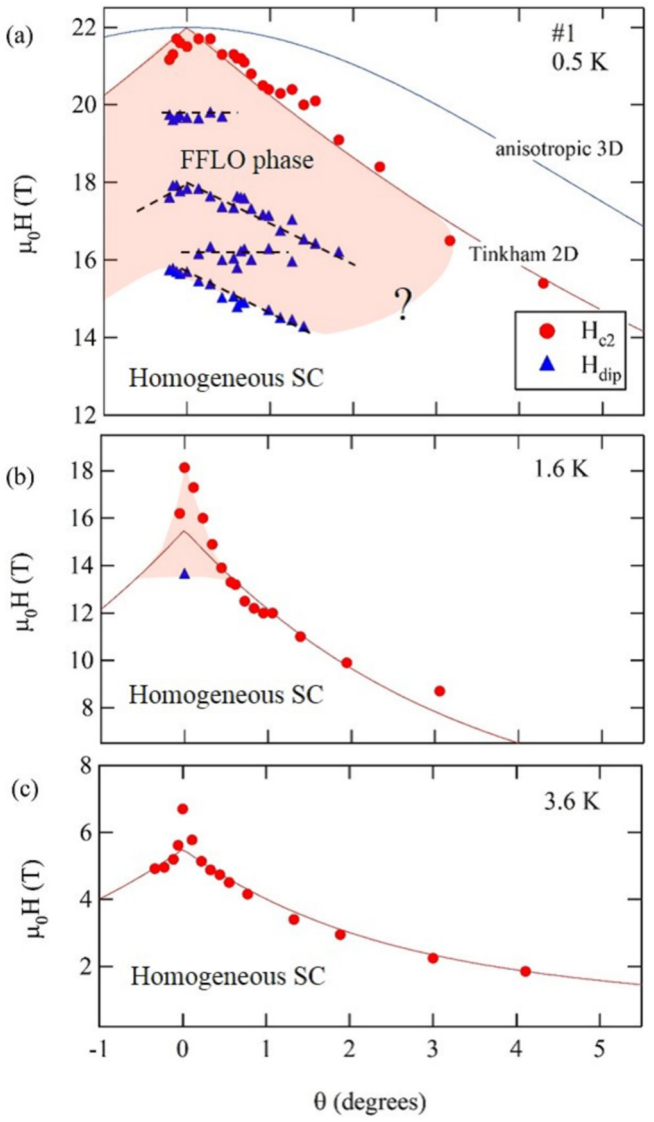

FIG. 7. Angular dependence of H_{c2} and $H_{\rm dip}$ at (a) 0.5 K, (b) 1.6 K, and (c) 3.6 K. Red and blue curves show the simulations for the Tinkham 2D and anisotropic 3D models, respectively. The parameters used for the simulations are: $H_{c2\perp} = 2.5$ T and $H_{c2\parallel} = 21.8$ T at 0.5 K, $H_{c2\perp} = 0.55$ T and $H_{c2\parallel} = 15.5$ T at 1.6 K, and $H_{c2\perp} = 0.15$ T and $H_{c2\parallel} = 5.5$ T at 3.6 K. Dotted curves are guides for the eye. Red shaded regions show the expected FFLO phases. The phase boundary at $\sim 3^\circ$ is unclear in (a).

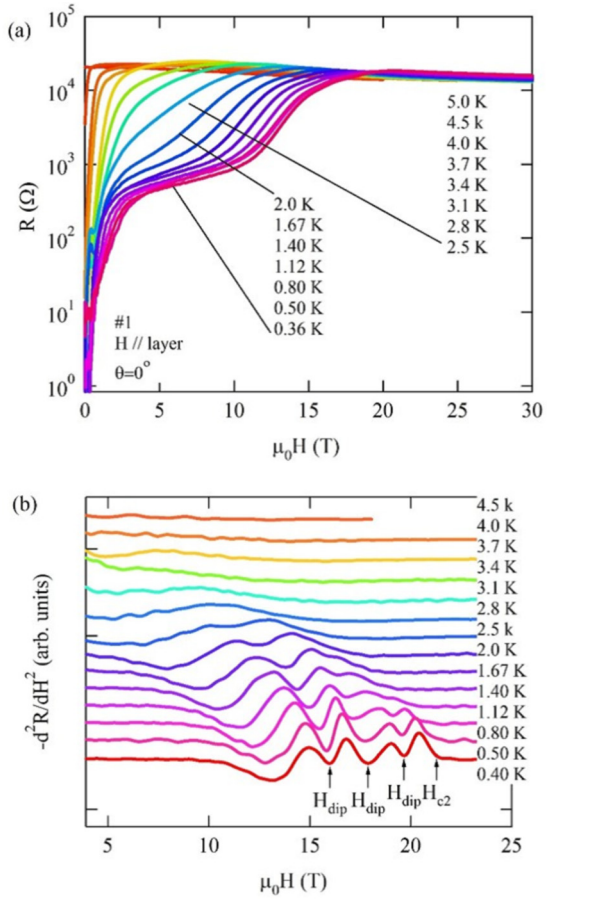

FIG. 8. (a) Semilog plot of the resistance at various temperatures in parallel fields. (b) Second derivative curves $-d^2R/dH^2$. The curves are shifted for clarity.

pinning in the SC layers. The average of the two-rotation curves gives the reversible part of the diamagnetic torque signal. In parallel fields ($\theta = 0^\circ$), we obtain no torque (no diamagnetism) because $M_\perp = 0$. The torque steeply decreases as the field is tilted from the layers. This diamagnetism ($-M_\perp \propto H_\perp$) means that most of the flux lines penetrate the insulating layers but not in the SC layers [11]. As the magnetic field is further tilted, the torque has a sharp dip (maximum of the diamagnetism) and then increases, showing that many flux lines start penetrating the SC layers. At a higher angle, the torque curve becomes reversible and then the SC state is completely broken. Figure 10 presents the averaged torque curves at various fields. The diamagnetic torque signal gradually decreases with increasing field. Even at $\sim$25 T, which is much larger than $H_{\rm irr}$, the diamagnetic signal is slightly observed, likely due to large SC fluctuations. Figure 11 presents the magnetic field dependence of the peak height $\Delta\tau_{\rm peak}$ of the averaged torque curve. The peak height, defined in the inset of Fig. 10, corresponds to the maximum diamagnetic signal. The kinks in Fig. 11 show the presence of a phase transition as discussed below.

IV. DISCUSSION

The phase diagram in parallel fields is presented in Fig. 12, where H_{c2} and $H_{\rm dip}$ from the resistance measurements, and $H_{\rm irr}$ and $H_{\rm kink}$ from the torque measurements are plotted. The irreversibility field $H_{\rm irr} = 21$ T at 0.5 K agrees with H_{c2}. The $H_{\rm kink}$ value coincides with H_{c2} at 3.6 K but is apparently lower than H_{c2} at 1.56 K and 0.4 K. In the FFLO phase, the flux lines will easily penetrate the SC layers along the nodal lines of the order parameter from the sample edges, which leads to the reductions of the diamagnetic torque signal. Therefore, the kinks of $\Delta\tau_{\rm peak}$ in Fig. 11 provide reasonable evidence of the FFLO phase boundary ($H_{\rm FFLO}$) as has been discussed in other layered organic superconductors [4,14].

The dips of the $-d^2R/dH^2$ curves show relatively strong pinning of the JVs at $H_{\rm dip}$. The origin of the dips will be ascribed to the CM effect between the wavelength of the FFLO

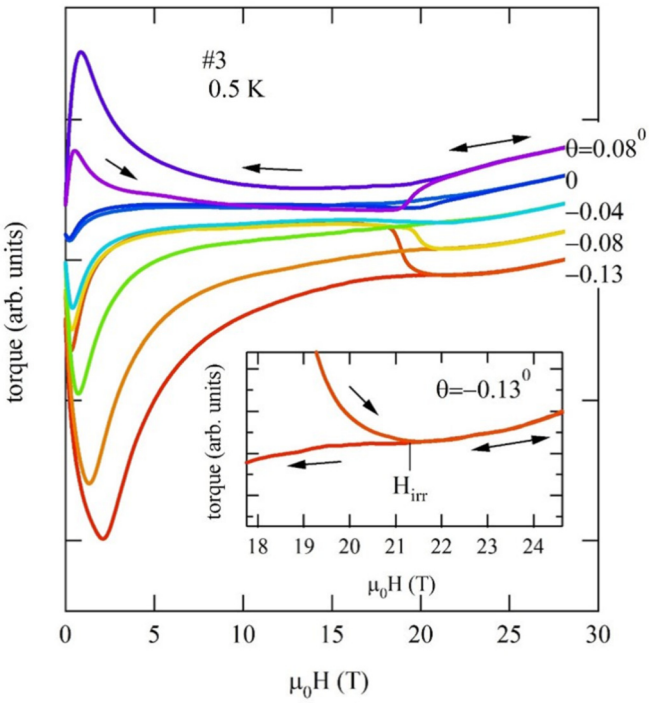

FIG. 9. Magnetic torque curves as a function of field in nearly parallel fields at 0.5 K. The curves are shifted for clarity. Inset: Closeup of the torque curve for $\theta = -0.13^\circ$. Large hysteresis due to vortex pinning is observed up to ~21 T, which is defined as the irreversibility field $H_{\rm irr}$.

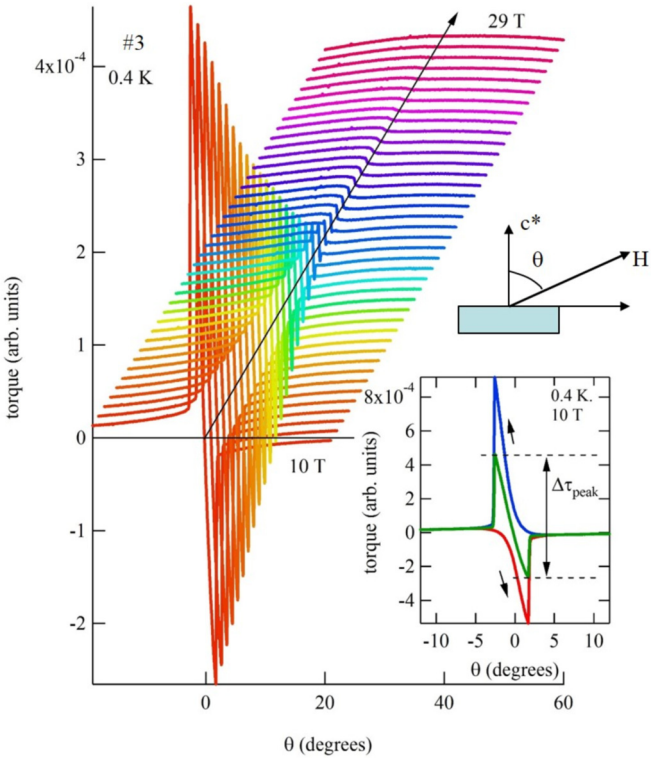

FIG. 10. Averaged torque curves at fields from 10 to 29 T with a step of 0.5 T. Inset: Typical torque curves for two different rotations (blue and red curves). The average of the two-rotation curves (green curve) corresponds to the reversible part of the diamagnetic torque signal without the pinning effect. The peak height $\Delta\tau_{\rm peak}$ is defined by the arrow.

order parameter oscillation $\lambda_{\rm FFLO}$ and the JV lattice constant l [4,25]. The lattice constant is given by $l = \Phi_0/sH$, where s is the layer spacing ($s = 1$ nm) and Φ_0 is the flux quantum. In the homogeneous SC phase, $\lambda_{\rm FFLO}$ is infinite, but expected to jump to a finite value at the FFLO transition. After that, $\lambda_{\rm FFLO}$ decreases with increasing field up to H_{c2}. It is theoretically difficult to obtain the optimum **q** vector for anisotropic Fermi surfaces such as the β"-salt [Fig. 3(b)] because the stability of the FFLO phase is closely related to the nesting condition of the Fermi surface [37]. For simplicity, we assume that the **q** vector is perpendicular to the field in the following discussion. As long as the q vector is not parallel to the field direction, our conclusion is qualitatively unaffected. As discussed in λ-$(BETS)_2FeCl_4$ [4], we also assume that the dips appear in the $-d^2R/dH^2$ curves when the ratios $m = l/\lambda_{\rm FFLO}$ are given by simple integers and it is close to unity at $H_{\rm FFLO}$ for simplicity. On these assumptions, we obtain $\lambda_{\rm FFLO}$ at 0.5 K on the right scale in Fig. 12. We can see an upward curvature of $\lambda_{\rm FFLO}$ with decreasing field. The same tendency can be obtained for other combinations of the number m. The $\lambda_{\rm FFLO}$ values obtained here are comparable to those in λ-$(BETS)_2FeCl_4$ [4].

Tachiki *et al.* theoretically discussed the SC order parameter of a FFLO phase, including the orbital current effect, and obtained the field dependence of $\lambda_{\rm FFLO}$ [38]. The $\lambda_{\rm FFLO}(H)$ curve has an upward curvature, ranging from $30\xi_\parallel$ to $13\xi_\parallel$ when the orbital effect is strongly suppressed. As the orbital effect increases, the FFLO field region shrinks. Shimahara theoretically estimated $\lambda_{\rm FFLO}$ for a 2D system and showed that $\lambda_{\rm FFLO}$ at H_{c2} decreases down to $\pi\xi_\parallel$ with decreasing temperature [37]. In Fig. 12, we obtain $\lambda_{\rm FFLO} = 3\xi_\parallel \sim 11\xi_\parallel$. In Fig. 7(a), the four series of the dips are found; two are independent of the angle and the others decrease with angle. Theoretically,

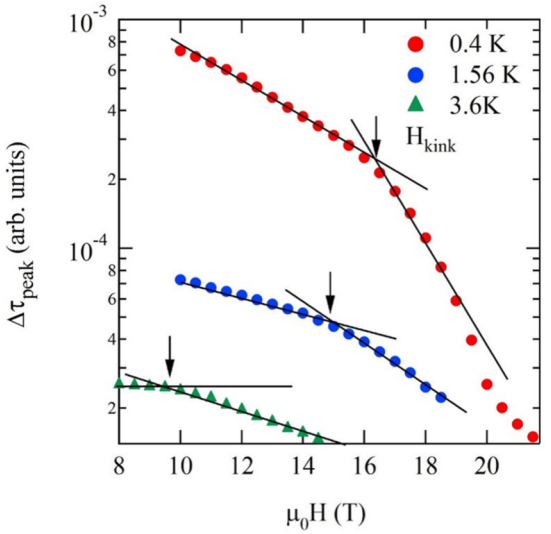

FIG. 11. Magnetic field dependence of the torque peak height $\Delta\tau_{\rm peak}$, defined in the inset of Fig. 10. Arrows indicate kinks in the field dependence, showing the reduction of the diamagnetic signal.

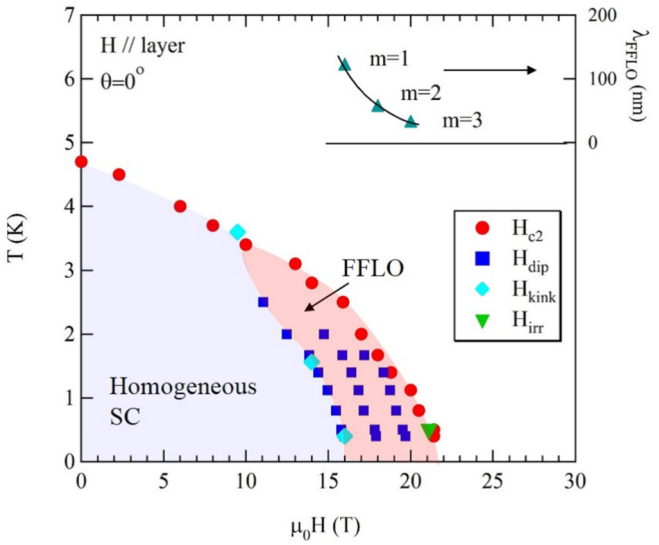

FIG. 12. Magnetic field phase diagram in parallel fields. H_{c2} and $H_{\rm dip}$ are determined from the resistance measurements, and $H_{\rm irr}$ and $H_{\rm kink}$ are from the torque measurements. The estimated wavelength of the FFLO order parameter oscillation, $\lambda_{\rm FFLO}$ at 0.5 K, is also shown on the right scale.

FFLO phases with multi **q** vectors are expected to appear at sufficiently low temperatures [39]. In such phases, the optimum **q** vectors will show complicated field dependence. At present, it is not clear whether a multi-**q**-vector phase is realized for the β"-salt. Further investigations will be required to understand the angular dependence of $H_{\rm dip}$.

In Fig. 7(a), $H_{\rm FFLO}$ seems to decrease as the field is tilted from the layer. The FFLO phase should be closed in the phase diagram; $H_{\rm FFLO}$ should merge with the H_{c2} curve. Such behavior is not seen in our experiments. Further studies are required to understand these results.

Table I presents the SC parameters for layered organic superconductors showing FFLO phase transitions. Among various superconductors, the CM effect has been observed for λ-$(BETS)_2FeCl_4$ and β"-salts. The $H_{c2\parallel}/H_{c2\perp}$ value is a good measure of the two dimensionality of the SC state. The CM effect will be observed when the JVs are collectively driven, which requires the weak Josephson coupling, highly 2D SC state. Therefore, the large $H_{c2\parallel}/H_{c2\perp}$ value in the β"-salt is consistent with the observation of the CM effect. β"-$(ET)_2SF_5CH_2CF_2SO_3$ is another good candidate for the CM effect.

In the weak coupling BCS theory, the energy gap at 0 K is given by $\Delta_0 = 1.76 k_B T_c$. Using the Pauli limit $H_{\rm Pauli} = \Delta_0/\sqrt{2}\mu_B$, we obtain $\mu_0 H_{\rm Pauli}/T_c = 1.84$ [T/K]. It is generally expected that the FFLO transition takes place at $\sim H_{\rm Pauli}$. Since these materials are probably non-s-wave superconductors, the weak coupling model is not directly applicable. However, we note that the $\mu_0 H_{\rm FFLO}/T_c$ values for most of the salts are comparable to 1.84 except 3.1 for the β"-salt. The reason of $H_{\rm FFLO} > H_{\rm Pauli}$ for the β"-salt will be closely related to the Fermi surface structure. The β"-salt has only small Fermi surfaces [Fig. 3(b)], whereas the others have a closed pocket and two sheets of Fermi surfaces with flat parts. The flat parts, which have a nesting instability, can form many Cooper pairs with a center-of-mass **q** vector in a FFLO phase. Therefore, the flat parts are more favorable for the FFLO phase transition and will give a lower $H_{\rm FFLO}$. The less flat parts of the Fermi surface for the β"-salt will lead to a relatively high $H_{\rm FFLO}$. By contrast, $H_{c2\parallel}$ will be mainly limited by the orbital effect, which is strongly suppressed for the β"-salt because of the large anion between the BEDT-TTF layers.

Finally we discuss the origin of the kink in the resistance curve at ∼13 T for $\theta = 0^\circ$ in Fig. 4. Nonzero resistance in a wide field region up to H_{c2} shows that JVs are easily driven by the perpendicular current. At low temperatures and small fields, the SC layers are strongly Josephson coupled [Fig. 1(a)]. As the field increases, the interlayer coupling weakens and then the layers will be decoupled. After the decoupling, the JV lattice in each layer can be driven independently. This decoupling, which effectively reduces the pinning force of the JVs, will increase the interlayer resistance. This is a possible mechanism of the kink at ∼13 T. As the field is tilted from the layer, the flux lines penetrate the SC layers and the pancake vortices are formed. This flux line structure will obscure the decoupling transition of the JV layers, as seen in Fig. 4. As the temperature increases, the kink field decreases [Fig. 8(a)]. The result is consistent with the above picture; the Josephson coupling is reduced with increasing temperature.

V. CONCLUSIONS

We have reported the resistance and magnetic torque measurements in the highly 2D organic superconductor, β"-(BEDT-TTF)$_4$[$(H_3O)Ga(C_2O_4)_3$]$C_6H_5NO_2$ with $T_c = 4.8$ K.

TABLE I. Superconducting parameters in layered organic superconductors. ET: BEDT-TTF; β"-salt: β"- $(BEDTTTF)_4$[$(H_3O)Ga(C_2O_4)_3$]$C_6H_5NO_2$; CE: commensurability effect; Ref.: references.

Material	T_c [K]	$\mu_0 H_{c2\perp}$ [T]	$\mu_0 H_{c2\parallel}$ [T]	$H_{c2\parallel}/H_{c2\perp}$	$\mu_0 H_{\rm FFLO}$ [T]	$\mu_0 H_{\rm FFLO}/T_c$ [T/K]	CE	Ref.
κ-$(ET)_2Cu(NCS)_2$	9.5 ∼ 10	7	28 ∼ 34	4 ∼ 4.8	21 ∼ 23	2.0 ∼ 2.2	none	[1,5,6,9,10,13,14]
λ-$(BETS)_2GaCl_4$	5 ∼ 5.7	4	12 ∼ 13	3 ∼ 3.3	9.5 ∼ 10	1.7 ∼ 2.0	none	[3,8,15]
λ-$(BETS)_2FeCl_4$	3 ∼ 4		16[a]		7[a]	1.8 ∼ 2.1	◯	[2,4,11,12]
β"-$(ET)_2SF_5CH_2CF_2SO_3$	4.7 ∼ 5.2	1.3	14	11.5	9.5-10	1.9 ∼ 2.1	[b]	[7,16]
β"-salt	4.8	2.5	21	8.4	15	3.1	◯	this work

[a]Estimated by considering the internal field [4].
[b]Not reported.

At 0.4 K in parallel magnetic fields, we observe nonzero interlayer resistance due to the JV dynamics in the wide field region. At ∼13 T, the resistance has the kink, which is likely due to the interlayer decoupling of the JVs. In the region between 16 T and H_{c2}, we observe the successive dips in the $-d^2R/dH^2$ curves. The dips, showing the relatively strong pinning of the JVs, are interpreted as the CM effect between the Josephson vortex lattice and the periodic order parameter oscillation of the FFLO phase. The magnetic torque curves associated with the large hysteresis show that the bulk superconductivity is evident up to 21 T, consistent with the resistance results. The significant reduction of the diamagnetic signal above ∼16 T shows the FFLO phase transition, consistent with the observation of the successive dips in the $-d^2R/dH^2$ curves between 16 T and H_{c2}. On the few assumptions, we obtain the field dependence of λ_{FFLO}, which ranges from $3\xi_{\parallel}$ at H_{c2} to $\sim 11\xi_{\parallel}$ at H_{FFLO}. The angular dependence of the dip field H_{dip} shows the four series; two are independent of the angle and the others decrease with angle. The behavior may suggest the possibilities of the complicated **q** vector phases in the FFLO phase.

ACKNOWLEDGMENTS

We acknowledge valuable discussions with S. Imajo (Osaka Univ.). This work was supported by a Grant-in-Aid for Scientific Research from MEXT, Japan (No. 17H01144). A portion of this work was performed at the National High Magnetic Field Laboratory, which is supported by National Science Foundation Cooperative Agreement No. DMR-1157490 and the State of Florida.

[1] J. Singleton, J. A. Symington, M.-S. Nam, A. Ardavan, M. Kurmoo, and P. Day, J. Phys.: Condens. Matter **12**, L641 (2000).
[2] L. Balicas, J. S. Brooks, K. Storr, S. Uji, M. Tokumoto, H. Tanaka, H. Kobayashi, A. Kobayashi, V. Barzykin, and L. P. Gorkov, Phys. Rev. Lett. **87**, 067002 (2001).
[3] M. A. Tanatar, T. Ishiguro, H. Tanaka, and H. Kobayashi, Phys. Rev. B **66**, 134503 (2002).
[4] S. Uji, T. Terashima, M. Nishimura, Y. Takahide, T. Konoike, K. Enomoto, H. Cui, H. Kobayashi, A. Kobayashi, H. Tanaka, M. Tokumoto, E. S. Choi, T. Tokumoto, D. Graf, and J. S. Brooks, Phys. Rev. Lett. **97**, 157001 (2006).
[5] R. Lortz, Y. Wang, A. Demuer, P. H. M. Bottger, B. Bergk, G. Zwicknagl, Y. Nakazawa, and J. Wosnitza, Phys. Rev. Lett. **99**, 187002 (2007).
[6] B. Bergk, A. Demuer, I. Sheikin, Y. Wang, J. Wosnitza, Y. Nakazawa, and R. Lortz, Phys. Rev. B **83**, 064506 (2011).
[7] K. Cho, B. E. Smith, W. A. Coniglio, L. E. Winter, C. C. Agosta, and J. A. Schlueter, Phys. Rev. B **79**, 220507 (2009).
[8] W. A. Coniglio, L. E. Winter, K. Cho, C. C. Agosta, B. Fravel, and L. K. Montgomery, Phys. Rev. B **83**, 224507 (2011).
[9] J. A. Wright, E. Green, P. Kuhns, A. Reyes, J. Brooks, J. Schlueter, R. Kato, H. Yamamoto, M. Kobayashi, and S. E. Brown, Phys. Rev. Lett. **107**, 087002 (2011).
[10] C. C. Agosta, J. Jin, W. A. Coniglio, B. E. Smith, K. Cho, I. Stroe, C. Martin, S. W. Tozer, T. P. Murphy, E. C. Palm, J. A. Schlueter, and M. Kurmoo, Phys. Rev. B **85**, 214514 (2012).
[11] S. Uji, K. Kodama, K. Sugii, T. Terashima, Y. Takahide, N. Kurita, S. Tsuchiya, M. Kimata, A. Kobayashi, B. Zhou, and H. Kobayashi, Phys. Rev. B **85**, 174530 (2012).
[12] S. Uji, K. Kodama, K. Sugii, T. Terashima, T. Yamaguchi, N. Kurita, S. Tsuchiya, M. Kimata, T. Konoike, A. Kobayashi, B. Zhou, and H. Kobayashi, J. Phys. Soc. Jpn. **82**, 034715 (2013).
[13] H. Mayaffre, S. Kramer, M. Horvatic, C. Berthier, K. Miyagawa, K. Kanoda, and V. F. Mitrovic, Nat. Phys. **10**, 928 (2014).
[14] S. Tsuchiya, J. Yamada, K. Sugii, D. Graf, J. S. Brooks, T. Terashima, and S. Uji, J. Phys. Soc. Jpn. **84**, 034703 (2015).
[15] S. Uji, K. Kodama, K. Sugii, T. Terashima, T. Yamaguchi, N. Kurita, S. Tsuchiya, T. Konoike, M. Kimata, A. Kobayashi, B. Zhou, and H. Kobayashi, J. Phys. Soc. Jpn. **84**, 104709 (2015).
[16] G. Koutroulakis, H. Kuhne, J. A. Schlueter, J. Wosnitza, and S. E. Brown, Phys. Rev. Lett. **116**, 067003 (2016).
[17] S. Uji, T. Terashima, T. Konoike, T. Yamaguchi, S. Yasuzuka, A. Kobayashi, and B. Zhou, Phys. Rev. B **95**, 165133 (2017).
[18] P. Fulde and R. A. Ferrell, Phys. Rev. **135**, A550 (1964).
[19] A. I. Larkin and Y. N. Ovchinnikov, Sov. Phys. JETP **20**, 762 (1965).
[20] H. Kobayashi, H. Tomita, T. Naito, A. Kobayashi, F. Sakai, T. Watanabe, and P. Cassoux, J. Am. Chem. Soc. **118**, 368 (1996).
[21] L. Brossard, R. Clerac, C. Coulon, M. Tokumoto, T. Ziman, D. K. Petrov, V. N. Laukhin, M. J. Naughton, A. Audouard, F. Goze, A. Kobayashi, H. Kobayashi, and P. Cassoux, Eur. Phys. J. B **1**, 439 (1998).
[22] H. Akiba, K. Nobori, K. Shimada, Y. Nishio, K. Kajita, B. Zhou, A. Kobayashi, and H. Kobayashi, J. Phys. Soc. Jpn. **80**, 063601 (2011).
[23] S. Uji, H. Shinagawa, T. Terashima, T. Yakabe, Y. Terai, M. Tokumoto, A. Kobayashi, H. Tanaka, and H. Kobayashi, Nature (London) **410**, 908 (2001).
[24] V. Jaccarino and M. Peter, Phys. Rev. Lett. **9**, 290 (1962).
[25] L. Bulaevskii, A. Buzdin, and M. Maley, Phys. Rev. Lett. **90**, 067003 (2003).
[26] H. Akutsu, A. Akutsu-Sato, S. S. Turner, D. L. Pevelen, P. Day, V. Laukhin, A.-K. Klehe, J. Singleton, D. A. Tocher, M. R. Probert, and J. A. K. Howard, J. Am. Chem. Soc. **124**, 12430 (2002).
[27] C. Rossel, P. Bauer, D. Zech, J. Hofer, M. Willemin, and H. Keller, J. Appl. Phys. **79**, 8166 (1996).
[28] A. I. Coldea, A. F. Bangura, J. Singleton, A. Ardavan, A. Akutsu-Sato, H. Akutsu, S. S. Turner, and P. Day, Phys. Rev. B **69**, 085112 (2004).
[29] A. F. Bangura, A. I. Coldea, J. Singleton, A. Ardavan, A. Akutsu-Sato, H. Akutsu, S. S. Turner, P. Day, T. Yamamoto, and K. Yakushi, Phys. Rev. B **72**, 014543 (2005).
[30] Y. Ihara, H. Seki, and A. Kawamoto, J. Phys. Soc. Jpn. **82**, 083701 (2013).
[31] Y. Ihara, M. Jeong, H. Mayaffre, C. Berthier, M. Horvatic, H. Seki, and A. Kawamoto, Phys. Rev. B **90**, 121106(R) (2014).

[32] Because of the software restriction [33], the band calculation was performed after a unit cell transformation from the C-centered lattice (x,y,z) to the primitive lattice $(x',y',z') = (z,0.5x + 0.5y, -x)$. The cell parameters are as follows; $a' = 3.5542$ nm, $b' = 1.1328$ nm, $c' = 1.0355$ nm, $\alpha' = 117.20^\circ, \beta' = 87.43^\circ, \gamma' = 91.18^\circ$, and $V = 3.7043$ nm^3.

[33] T. Mori, A. Kobayashi, Y. Sasaki, H. Kobayashi, G. Saito, and H. Inokuchi, Bull. Chem. Soc. Jpn. **57**, 627 (1984).

[34] M. Tinkham, Phys. Rev. **129**, 2413 (1963).

[35] E. I. Kats, Sov. Phys. JETP **29**, 897 (1969).

[36] J. C. Martinez, S. H. Brongersma, A. Koshelev, B. Ivlev, P. H. Kes, R. P. Griessen, D. G. de Groot, Z. Tarnavski, and A. A. Menovsky, Phys. Rev. Lett. **69**, 2276 (1992).

[37] H. Shimahara, Phys. Rev. B **50**, 12760 (1994).

[38] M. Tachiki, S. Takahashi, P. Gegenwart, M. Weiden, M. Lang, C. Geibel, F. Steglich, R. Modler, C. Paulsen, and Y. Onuki, Z. Phys. B **100**, 369 (1996).

[39] H. Shimahara, J. Phys. Soc. Jpn. **67**, 736 (1998).